



Effect of pH on the Corrosion Behavior of Aluminium Alloy Welded Plate in Chloride Solutions

Venkatasubramanian G.¹, Sheik Mideen A.^{1*} and Aboy K. Jha²

¹Department of Chemistry, Sathyabama University, Jeppiaar Nagar, Chennai-600119, INDIA

²Materials Characterization Division, Vikram Sarabhai Space Centre, Indian Space Research Organisation, Trivandrum, INDIA

Available online at: www.isca.in

Received 24th May 2013, revised 30th May 2013, accepted 15th June 2013

Abstract

The corrosion behavior of aluminium alloy AA2219–T87 gas tungsten arc welded (GTAW) plates in 0.6M NaCl solution at pH 6.5 and at pH 10 was investigated using potentiodynamic polarization and electrochemical impedance spectroscopic (EIS) techniques. The surface morphology of the welded plates was characterized by optical microscopy, scanning electron microscopy with energy dispersive x-ray analysis (EDX). The electrochemical measurements showed that the heat affected zone (HAZ) is more susceptible to general corrosion as well as pitting corrosion in near neutral and in alkaline NaCl solution when compared to the weld zone (WZ) and to the base metal (BM). The EDX analysis further revealed the segregation of CuAl₂ intermetallic particles along the grain boundaries due to the welding heat temperature and is responsible for higher corrosion rate of HAZ. The charge transfer resistance obtained from EIS study confirmed the active dissolution of HAZ in alkaline NaCl solution than in near neutral NaCl solution.

Keywords: Aluminium, EIS, SEM, HAZ, EDX

Introduction

The investigation of corrosion and its inhibition of aluminum/aluminum alloys in various environments¹⁻³ has great importance in aeronautical and automobile industries. Among the various aluminium alloys, 2xxx, 6xxx and 7xxx series are heat treatable commercial wrought alloys used in aerospace applications⁴⁻⁵. Particularly AA2219 has high strength and the most readily weldable⁶ and finds extensive use for the construction of cryogenic fuel tanks. But its main disadvantage is its poor corrosion resistance especially in chloride containing environment owing to higher copper content. The copper distribution in the microstructure affects the susceptibility to localised corrosion^{7,8}. Pitting corrosion is defined as “localized accelerated dissolution of metal that occurs as a result of a breakdown of the protective passive film on the metal alloy surface”⁹.

Aluminium alloys used for aerospace application are fabricated by various welding methods causes the physical, chemical and metallurgical changes in their microstructures. Welds can be made with the addition of filler metal or can be made autogenously (without filler metal). TIG welding process is commonly used to join AA2219 plates due to its inherent advantages of arc cleaning¹⁰. Welds in Al-Cu alloys such as AA2014¹¹, AA2219^{12,13} have been reported in which heat affected zone (HAZ) showed less corrosion resistance due to its cathodic nature to the remainder of the weldment. However, the investigation carried out by Balasrinivasan et al¹⁴ reported that the BM AA2219 showed poor corrosion resistance in 3.5% NaCl solution than WZ and HAZ. The effect of heat treatment on AA2219 also plays a vital role in the pitting and general

corrosion resistance of and the results showed that the T-87 temper condition was found to be better than T6 temper¹⁵.

The general corrosion behaviour of different regions of TIG welded plate was compared with repair welded AA2219-T87 plate in 3.5% NaCl with neutral pH using potentiodynamic polarization technique¹⁶. Pitting corrosion of AA2014 base metal was compared with GTA and FSW in O and T4 condition by Venkataramana et al¹⁷ in 3.5% NaCl at pH 10. Pitting potential of BM at O condition was found as -633mV but at T4 condition it was found as -600mV. Better pitting corrosion resistance of base metal at T4 condition is attributed to the copper enrichment at the grain boundary of the alloy in O condition. Pitting corrosion behaviour of friction stir welded AA2219 at different conditions in different corrosive environments was also investigated and reported by changing the processing parameters like different rotation speed and traverse speed^{18,21}. The welding processes like continuous current (CC), pulsed current (PC), arc oscillation (AO), combination of PC and AO welds have been used for welding of AA2219 and its corrosion behaviour was compared with EB welds²². Combination of PC and AO technique in GTAW of 2219 significantly reduced the segregation of copper resulting in better pitting corrosion resistance over the CC welds.

The present work elucidates the general and pitting corrosion behaviour of different zones namely, weld zone (WZ) and heat affected zone (HAZ) of gas tungsten arc welded AA2219–T87 plates in 0.6M NaCl at near neutral and higher pH(10) and compared the results with base metal (BM) in T87 temper condition.

Material and Methods

Gas tungsten arc welded (GTAW) AA2219 rolled plate of size 570mm × 500mm × 7.4mm in T-87 temper condition was used in the present study. The welding procedure used for joining the AA2219-T87 plates is described elsewhere²³. The chemical composition of base metal and filler wire are given in table-1.

The working electrodes for corrosion studies were cut from the welded plates parallel to the rolling direction and perpendicular to welding direction in such a way the test specimens consisted of base metal (BM), weld zone (WZ) and heat affected zone (HAZ). The working electrodes were soldered with Cu-wire for electrical connection and were embedded in epoxy resin. Figure-1 shows the flat type working electrode with all regions. The specimens were used in flat type with mirror smooth finish after mechanically abraded with different grades of silicon carbide sheets followed by 1 μm finish using rotating disc with non-aqueous diamond paste, degreased by acetone, washed with double distilled water and dried.

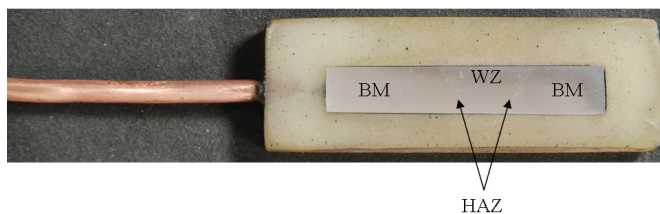


Figure-1

Locations of test specimens of base metal (BM), heat affected zones (HAZ) and weld zone (WZ)

Except the zone under study, the rest of the zones were suitably masked with a red lacquer and further wrapped with Teflon tape. The Keller etchant [2.5ml HNO₃ (60%) + 1.5ml HCl (37%) + 1ml HF (48%) + 95 ml of double distilled water] was used to identify the HAZ and are located 3 mm away from weld zones on both sides. In all experiments 8mm×1mm was exposed in order to compare the results.

Potentiodynamic polarization tests were carried out according to ASTM standard G3-89 (ASTM G3-89, 2004) using software based Bio-analytical system [BAS-Zahner, make IM6-electrochemical analyzer model using THALAS-Flink software]. The flat type working electrodes were categorized into BM, WZ and HAZ. A saturated calomel electrode coupled to a fine Luggin capillary as reference electrode and graphite

electrode as counter electrode were used. The Luggin capillary was kept close to the working electrode to reduce the ohmic contribution. Freshly prepared 0.6 M NaCl(pH 6.5) was used as electrolyte to investigate the general corrosion while the same solution, adjusted to pH 10 using 0.1M KOH was used to evaluate the pitting corrosion behaviour of AA2219-T87 welded plates.

The Tafel plot was obtained by stepping the potential at a scan rate of 0.5mV/sec from -250 mV (SCE) to +250 mV(SCE) vs OCP to find the E_{corr} and i_{corr} of different zones of AA2219-T87 welded plates in 0.6M NaCl at pH 6.5. In order to investigate the passive behaviour of AA2219-T87 welded plate, the potentiodynamic polarisation was carried out at pH 10 by stepping the potential at a scan rate of 0.5mV/sec from -1.4V (SCE) to -0.4V (SCE). The breakage of passive film was obtained by E_{pit}(pitting potential) and hence the corrosion current increases drastically with the further applied potential. All the experiments analyzed in this paper were performed at room temperature (25°C) and repeated for at least two times to get reproducibility.

The electrochemical impedance spectroscopy (EIS) measurements were carried out in 0.6 M NaCl at pH 6.5 and at pH 10 using a potentiostat coupled to a frequency response analyzer system in the frequency range 100 k Hz. to 100 m Hz. with amplitude of 10 mV peak to peak using AC signals at open circuit potential. The working electrode consists of either BM or WZ or HAZ, graphite electrode and saturated calomel electrode were used as counter electrode and reference electrode respectively. Potentiodynamic polarization and EIS measurements were performed after initial delay of 10 minutes for the sample to reach a steady state condition.

The microstructure of the AA2219-T87 welded plates were characterized by using optical microscopy (Olympus GX 71 Inverted Metallurgical Microscope, Japan) and Scanning Electron Microscopy (HITACHI 15kV). For optical metallography and SEM analysis the samples were cut in the transverse cross section and mechanically abraded with different grades of silicon carbide sheets followed by 1μm finish using rotating disc with non-aqueous diamond paste. Then the samples were degreased with acetone and etched with Keller's etchant for about 30 to 60 seconds.

Table-1
Nominal composition of AA2219-T87 GTA welded plate

Alloy	Elements							
	Cu	Mn	Zr	V	Ti	Fe	Si	Al
AA2219	5.95	0.27	0.12	0.09	0.06	0.05	0.05	Balance
ER2319	6.1	0.29	0.15	0.1	0.15	0.1	0.04	Balance

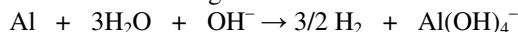
Results and Discussion

Potentiodynamic polarization: The potentiodynamic polarization curves for BM, WZ and HAZ of AA2219-T87 welded plate in 0.6M NaCl at pH 6.5 and 10 are shown in figure-2 and figure-4 respectively. The various corrosion parameters obtained from these plots are represented in table-2.

The BM, WZ and HAZ in 0.6M NaCl at pH 6.5 showed the open circuit potential(OCP) values of -683 mV, -663mV and -678 mV respectively. These values mainly depend upon the chemical composition and the dissolution of copper and CuAl₂ due to thermal temper and welding heat temperature of alloys. It is observed from the figure 2 that the regions like WZ and HAZ of AA2219 welded plate showed cathodic control reaction; since they have cathodic Tafel slopes higher than anodic Tafel slopes. The predominance of cathodic slope is due to the presence of main alloying element copper. The E_{corr} for BM when compared to WZ and HAZ exhibits a shift towards anodic side from OCP (-615mV). This shift was also confirmed in the reduction of corrosion current, 0.96μA/cm². This phenomena may be due to higher anodic to cathodic area distribution²⁴. The corrosion potential for WZ and HAZ shifts towards anodic side from OCP. This shift indicates that corrosion of these regions follow via anodic dissolution mechanism. This factor is further supported by corrosion current density (i_{corr}), which is 2.98μA/cm² for WZ and 6.8μA/cm² for HAZ. During welding, the temperature in these zones varies from 490 to 548°C²⁴. Due to this welding heat, a change in microstructures in these regions might have produced which in turn cause the changes in corrosion properties relative to that of BM. Considering the E_{corr} in neutral 0.6M NaCl solution, the segregation of CuAl₂ particle along the grains and presence of micro pores in HAZ and WZ respectively cause the shifting of corrosion potential towards the nobler side when compared to BM²⁵.

The open circuit potentials for the regions of BM, WZ and HAZ in 0.6M NaCl at pH 10 showed the values -1188mV, -1046mV and -1006mV respectively. The higher pH modifies the surface of aluminium alloy and shifts the OCP to more cathodic side when compared to 0.6M NaCl solution at pH 6.5. In the alkaline solutions, the passive film, AlO₂⁻ on aluminum and its alloys is unstable²⁶ and hence the matrix surface exposed to the solution leads to higher corrosion rate. The E_{corr} values observed for the regions of BM, WZ and HAZ in 0.6M NaCl at pH 10 are -911mV, -1002mV, -927mV respectively. The alkaline NaCl solution causes the E_{corr} of all the zones of the alloy towards negative side when compare to the near neutral solution. This negative shift in E_{corr} at higher pH may be due to the active dissolution of intermetallic particles followed by the redeposition of copper in turn caused the pitting corrosion of matrix¹². The increase in corrosion current density of all the zones of the alloy is due to the existence of AlO₂⁻ ions in alkaline solution rather than aluminum precipitation as Al(OH)₃ in near neutral solution²⁷. The change in slope of the cathodic polarization curve with pH of the test environment is attributed

to the change in the cathodic reaction at different pH levels²⁸. In alkaline solution the corrosion of Al proceeds mainly by water reduction according to the reaction:



In neutral solution, however, oxygen reduction will be the main cathodic reaction. In the present work, the oxygen concentration in the NaCl solution in addition to the high availability of OH⁻ ions at pH 10 is believed to be the reason for the change in slope of the cathodic polarization curves and the higher cathodic current densities observed in the alkaline solution. The acceleration of the cathodic reaction and the unstable nature of the passive film in the alkaline NaCl solution favour the negative shift in E_{corr} when the pH of the solution increases from 6.5 to 10. The anodic branch of potentiodynamic polarisation curves in 0.6M NaCl at pH 10 showed passive behaviour for all zones which is attributed to the negative shift in E_{corr}. Samples exhibiting a more positive potential were considered to have better pitting corrosion resistance. It is observed from fig. 4 that the pitting potential values were found to be -505mV, -552mV and -593mV for BM, WZ and HAZ respectively. It can be concluded from these data that the pitting corrosion resistance of HAZ was poorer than WZ and BM. This is also in well agreement with the previous results obtained from Tafel plots at 0.6M NaCl at 6.5 pH solution. The higher i_{corr} value for HAZ region in 0.6M NaCl at pH 6.5, and lower E_{pit} value for HAZ in 0.6MNaCl at pH 10 showed that it has low corrosion resistance than WZ and BM. This may be due to (i) complete dissolution and distribution of CuAl₂ particles along grain boundaries²⁹ and (ii) Segregation of copper from matrix by the welding heat and by thermal temper. This phenomena favour the formation of huge number of galvanic cells with respect to grain matrix and accelerate the rate of corrosion of HAZ region³⁰. The presence of copper in α-matrix and micro pores is responsible for the higher corrosion rate in WZ when compared to BM.

Electrochemical Impedance Spectroscopy: The Nyquist plots, Bode impedance and Bode phase plots corresponding to the AA2219-T87 aluminium alloy (BM) with different zones (WZ and HAZ) exposed in 0.6M NaCl solution at pH 6.5 and at pH 10 is presented in figure-3a-c and figure-5a-c respectively. The various corrosion parameters obtained from Nyquist plots for different zones of AA2219-T87 in 3.5% NaCl solution at different pH are presented in table-3. The low-frequency impedance of the corroded sample can be used a measure of the corrosion activity and the diameter of semicircle corresponding to charge transfer resistance (R_{ct}), was used to measure corrosion rate. The low diameter of Nyquist plot, higher impedance obtained from Bode impedance curve and broad phase angle confirm the active dissolution of HAZ in 0.6M NaCl both at pH 6.5 and 10. The Nyquist plot obtained for AA2219-T87 welded plate exposed to 0.6M NaCl at pH 10 showed two semi circles indicating that all the zones of the alloy exhibit the passive regions. It has been observed from the Table 3 that the charge transfer resistance (R_{ct}) follows the order BM>WZ>HAZ in 0.6M NaCl solution of pH 6.5 as well as in

0.6M NaCl solution of pH 10. It is further supported by the increase of their double layer capacitance and decrease of impedance values. The lower charge transfer resistance and the higher double layer capacitance of all the zones of AA2219-T87 welded plate favour more corrosion in alkaline solution of 0.6M NaCl than in 0.6M NaCl solution of pH 6.5. The heat treatment followed by age hardening dissolve the majority of CuAl_2 particles into fine precipitates, eutectic enrichment and segregation of alloying element copper along elongated grain boundaries lead to extensive corrosion damage in HAZ when compared to BM and WZ. Presence of shrinkage pores and copper rich phase in WZ and selective dissolution along grain boundaries is responsible for its lower R_{ct} .

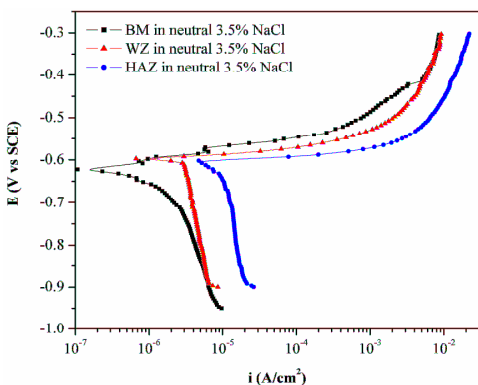


Figure-2

Anodic and cathodic polarization curves for different zones of AA 2219-T87 welded plate in 0.6M NaCl solution at pH 6.5

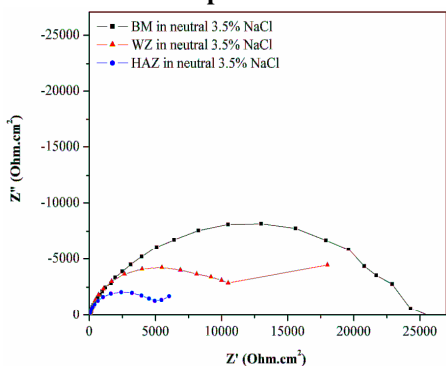


Figure-3a

Nyquist plot for different zones of AA2219-T87 welded plate in 0.6M NaCl solution at pH 6.5

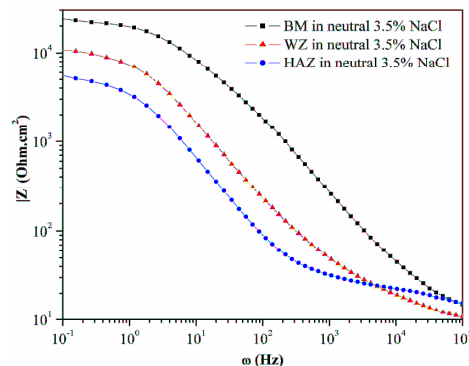


Figure-3b

Bode Impedance plots for different zones of AA2219-T87 welded plate in 0.6M NaCl solution at pH 6.5

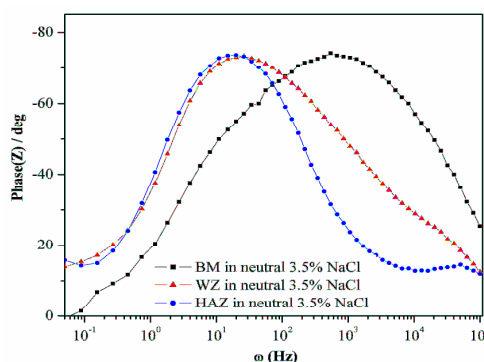
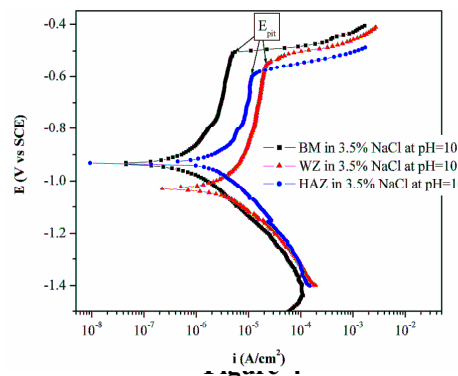


Figure-3c

Bode phase plots for different zones of AA2219-T87 welded plate in 0.6M NaCl solution at pH 6.5



Anodic and cathodic polarization curves for different zones of AA2219-T87 welded plate in 0.6M NaCl solution at pH 10

Table-2

Corrosion parameters obtained from Tafel plots for the corrosion behaviour of AA2219-welded plate in 0.6M NaCl solution at pH 6.5

Sl. No.	Various zones of AA2219-T87 welded plate in 0.6M NaCl at pH 6.5	i_{corr} ($\mu\text{A}.\text{cm}^{-2}$)	β_a (mV.dec-1)	β_c (mV.dec-1)	E_{corr} mV vs SCE
1	BM	0.960	33.5	-410.7	-615
2	WZ	2.98	22.9	-848	-603
3	HAZ	6.8	22.1	-730	-609

Table-3
Impedance parameters for different zones of AA 2219-T87 welded plate in 0.6M NaCl at pH 6.5 and 10

Sl. No.	Various zones of AA2219-T87 welded plate	R_{ct} ($k\Omega.cm^{-2}$)	C_{dl} ($\mu F.cm^{-2}$)	Z ($k\Omega.cm^{-2}$)
1	BM in 3.5% NaCl pH 6.5	28	1.5×10^{-3}	23.6
2	WZ in 3.5% NaCl pH 6.5	14	6.5×10^{-3}	10.6
3	HAZ in 3.5% NaCl pH 6.5	5.8	1.5×10^{-2}	5.4
4	BM in 3.5% NaCl pH 10	5.9	1.4	14.2
5	WZ in 3.5% NaCl pH 10	2.2	10	5.9
6	HAZ in 3.5% NaCl pH 10	1.4	16.2	5.3

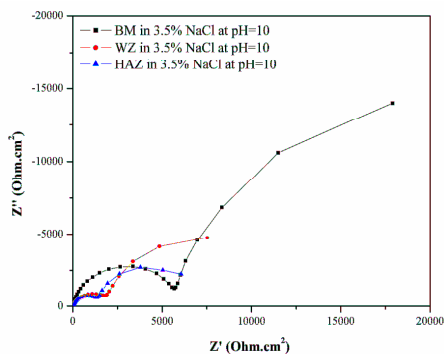


Figure-5a

Nyquist plot for different zones of AA2219-T87 welded plate in 0.6M NaCl solution at pH 10

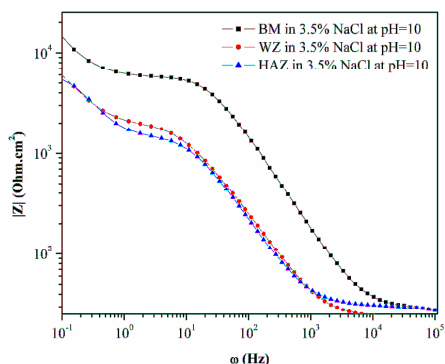


Figure-5b

Bode Impedance plots for different zones of AA2219-T87 welded plate in 0.6M NaCl solution at pH 10

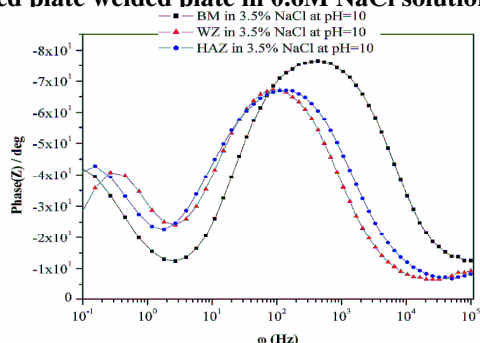


Figure-5c

Bode phase plots for different zones of AA2219-T87 welded plate in 0.6M NaCl solution at pH 10

Microstructure analysis: The distribution, location, size, quantity and corrosion potential of $CuAl_2$ intermetallic particles relative to the adjacent α -Al matrix is the important aspect of corrosion behavior²². Figure-6a shows the microstructure of BM, consisting of elongated grains in α phase with uniform distribution of $CuAl_2$ intermetallic particles⁶. Figure-6b shows the SEM-EDX analysis of intermetallic particles and matrix phase of BM. The Al/Cu weight ratio of these particles was close to 53/47 for $\theta(CuAl_2)$ ³¹ and the matrix phase contains Al/Cu weight ratio 90/7. The presence of $CuAl_2$ particles in α -solid solution and the solute element copper forms micro galvanic cells with surrounding matrix³² are responsible for the corrosion of BM in both electrolytes.

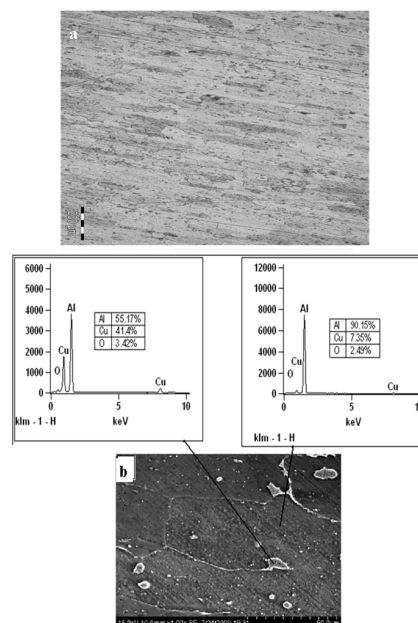


Figure-6

(a) Microstructure (b) SEM-EDX image of base metal

Figure-7a shows the microstructure of weld zone consisting of a population of more copper rich areas (dark) in α -solid solution than the BM. SEM micrograph of WZ (figure-7b) exhibits a randomly distributed shrinkage pores and copper. The presence of copper in α -matrix and micro pores is responsible for the higher corrosion rate of WZ. Figure-7b shows the SEM-EDX analysis of enriched copper in the IMPs rather than the matrix.

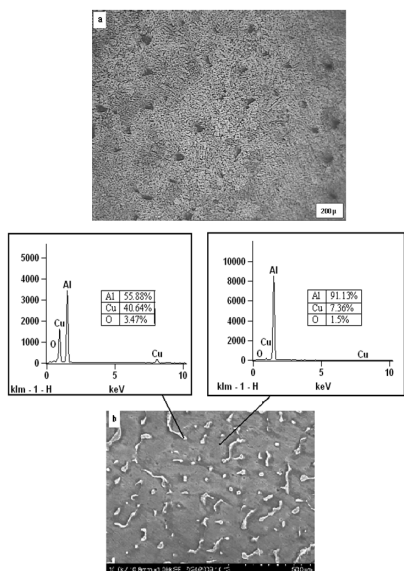


Figure-7

(a) Microstructure (b) SEM-EDX image of weld zone

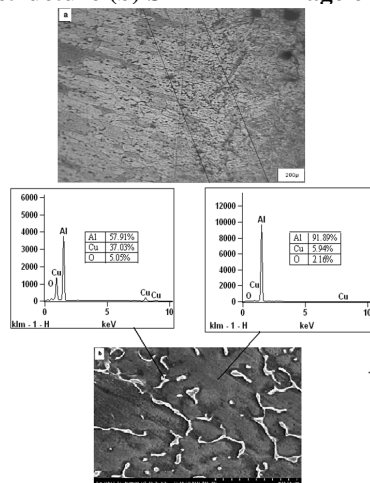


Figure-8

(a) Microstructure (b) SEM-EDX image of heat affected zone

Figure-8a shows the microstructure of HAZ. The SEM micrograph of HAZ (figure-8b) clearly shows more segregation of CuAl_2 intermetallic particles along the grain boundaries. Before welding the AA2219 consists of an aluminium rich matrix, α -Al and numerous θ , CuAl_2 particles in it. During welding, the temperature in HAZ varies from 490°C to 548°C (eutectic temperature). Due to this welding temperature the fine θ precipitates dissolve and segregate along grain boundaries as higher dense precipitates and remain after cooling. The increasing fraction of CuAl_2 particles at the grain boundaries increases the susceptibility to corrosion action with respect to grain matrix³¹. Figure-8b shows SEM-EDX image of HAZ with the increased amount of CuAl_2 particles compared to the matrix. The increased rate of corrosion of HAZ is due to the selective dissolution of copper rich intermetallic particles in both electrolytes.

Conclusion

The corrosion behavior of AA2219-T87 GTA welded plate has been investigated in near neutral and in alkaline chloride containing solutions by electrochemical techniques. The general and pitting corrosion resistance of different zones of AA2219-T87 welded plates in 0.6M NaCl solution at different pH follow the order: $\text{BM} > \text{WZ} > \text{HAZ}$. The shift in corrosion potential towards nobler side for HAZ and WZ decreases their corrosion resistance in near neutral solution due to the presence of Cu rich phases when compared to BM. The shift in corrosion potential in the negative side and change in cathodic slope of the Tafel plots indicates lower pitting resistance of HAZ when compared to WZ and BM are due to the active dissolution of intermetallic particles followed by the redeposition of copper in alkaline chloride solution. The results of the microstructural characterisation confirmed that the increased rate of corrosion of HAZ in both environments is due to the selective dissolution of more copper rich intermetallic particles than WZ and BM. On the other hand, the presence of copper in α -matrix and micro pores is responsible for the higher corrosion rate of WZ and BM respectively.

References

1. Bogar F.D. and Foley R.T., The Influence of Chloride Ion on the Pitting of Aluminium, *J. Electrochem. Soc.*, **119**, 462 (1974)
2. Sharma Pooja, Upadhyay R.K. and Chaturvedi Alok, A comparative study of corrosion inhibitive efficiency of some newly synthesized Mannich bases with their parent amine for Al in HCl solution, *Res. J. Chem. Sci.*, **1(5)**, 29-35 (2011)
3. Dubey J., Jeengar N., Upadhyay R.K., Chaturvedi A, Corrosion Inhibitive Effects of Withania Somnifera (A medicinal plant) on Aluminium in HCl Solution, *Res. J. Recent. Sci.*, **(1)**, 73-78 (2012)
4. Corrosion and Corrosion Protection Handbook, Schweitzer P.A., Marcel Dekker, Inc. (1983)
5. Chawla S.L. and Gupta R.K., Materials Selection for Corrosion Control, ASM International. 159-211 (1993)
6. Properties of Aluminium and Aluminium alloys, Metals Hand Book, 10th Ed. 2, 79-80 (1990)
7. Perkins J., Cummings J.R., and Graham K.J., *J. Electrochem. Soc.*, **129**, 137 (1982)
8. Lunarska E., Trela E., and Z. Szklarska-smialowska Z, Pitting corrosion of powder metallurgy AlZnMg alloy, *Corrosion*, **43(4)** 219-228 (1987)
9. Frankel G.S, Pitting corrosion of metals: A review of the critical factors, *J. Electrochem Soc.*, **(145)** 2186 (1998)
10. Ghosh, B. R.; Gupta, R. K.; Biju, S.; Sinha, P. P. Modified welding technique of a hypo-eutectic Al-Cu alloy for higher

- mechanical properties, *J. Solid Mechs. and Mater. Engg.*, (4)1, 469-479(2007)
11. Reed R.P., Aluminium alloys for ALS cryogenic tanks: Comparative measurements of Cryogenic mechanical properties of Al-Li alloys and alloy 2219, Philips Laboratory, Report TR-91- 3037, CA, (1991)
 12. Venkatasubramanian .G, Sheik Mideen .A, Abhay K Jha, Corrosion Behavior of Aluminium Alloy AA2219-T87 Welded Plates in Sea Water, *Indian Journal of Science and Technology*, (5) 11, 3578-3583(2012)
 13. Venkatasubramanian G., Sheik Mideen A., Abhay K. Jha, Microstructural characterisation and corrosion behaviour of top surface of TIG welded 2219-T87 aluminium alloy, *International Journal of Engineering Science and Technology*, (5)3, 624-629 (2013)
 14. Balasrinivasan P., Arora K.S., Ditzel W., Paney S., Schaper M.K, Characterization of microstructure, mechanical properties and corrosion behavior of an AA2219 friction stir weldment, *Journal of alloys and compounds*, 492(1-2), 631-637 (2010)
 15. Srinivasa Rao K. and Prasad Rao K., Corrosion resistance of AA2219- aluminium alloy; electrochemical polarisation and impedance study, *Material science and technology*, (22), 97-104 (2006)
 16. Venugopl A., Sreekumar K and Raja V.S., Effect of repair welding on electrochemical corrosion and stress corrosion cracking behavior of TIG welded AA2219 aluminium alloy in 3.5% Wt Pct NaCl solution, *Metallurgical and Materials transactions A*, (41A), 3151-3160(2010)
 17. Venkataramana V.S.N., Ratna kumar K., Madhusudhan Reddy G., and Sinivasa rao K, Effect of welding Process on microstructure and pitting corrosion behavior of AA2014 Al-Cu alloy welds, *IW-Welding journal*, (45) 3, 29-40 July (2012)
 18. Surekha K., Murthy B.S., Prasad Rao K., Effect of processing parameters on the corrosion behavior of friction stir processed AA2219 aluminium alloy, *Solid state science*, (11) 907-917(2009)
 19. Weifeng Xu, Jinhe Liu, Microstructure and pitting corrosion of friction stir welded joints in 2219-O aluminum alloy thick plate, *Corr. Sc.*, (51) 2743-2751(2009)
 20. Weifeng Xu, Jinhe Liu, Hongqiang Zhu, Pitting corrosion of friction stir welded aluminum alloy thick plate in alkaline chloride solution, *Electrochimica acta*, (55)2918-1923(2010)
 21. Koteswara rao S.R., Madhusudhan reddy G., Srinivasa rao K., Kamaraj. M, .Prasad Rao K., Reasons for superior mechanical and corrosion properties of 2219 aluminum alloy electron beam welds, *Materials characterization* (2005)
 22. Koteswara rao S.R., Srinivasa rao .K., Prasad rao K., Fusin zone grain refinement and its effect of pitting corrosion of 2219 aluminium alloy welds, Chennai,990-996 IIW-IC2008
 23. Venkata Narayana, G., Sharma V. M. J., Diwahar V, Sreekumar K, Prasad R. C. Fracture behaviour of aluminium alloy 2219- T87 welded plates, *Sci. and Tech. of Weld. and Joining*, (9)2 121-130(2004)
 24. Schonberg W.P., Aluminium 2219-T87 and 5456-H116: A comparative study of spacecraft wall materials in dual-wall structures under hypervelocity impact, *Acta Astronautica*,(26)11 799-812(1992)
 25. Reboul M., Meyer P., in Proceedings of the fourth International Aluminium-Lithium Conference, Vol. II, (edited by G. Champier, B. Dubost, D. Mianny and L. Sabetay), France, 10-12 June (1987)
 26. Pourbaix M, 'Atlas of Electrochemical Equilibrium Diagrams in Aqueous Solutions', NACE, Houston, Texas 499(1966)
 27. El-Menshawy K., El-Sayed .A.A., El-Bedawy M.E., Ahmed H. A., El-Raghy S.M, Some Corrosion Characteristics of Aged Aluminum Alloy 6061 in Neutral and Alkaline Solutions, *Arab Journal of Nuclear Sciences and Applications*, 45(2)51-59(2012)
 28. Dwarakadasa E.S., Studies on the influence of chloride ion and pH on the electrochemical behavior of aluminum alloys 8090 and 2014, *J. Applied Electrochemistry* (24) 911-916 (1994)
 29. Wang L., Makhlof M., Apelian D., Aluminium die casting alloys: alloy composition, microstructure, and properties-performance relationships, *Int. Mater. Rev.* (40) 221-238(1995)
 30. Osório W.R., Spinelli J.E., Boeira A.P., Freire C.M., Garcia A., The influences of macro segregation, intermetallic particles, and dendritic spacing on the electrochemical behavior of hypoeutectic Al-Cu alloys, *Micros. Res. and Techniq.* 70(11) 928-937 (2002)
 31. Srinivasa Rao K and Prasad Rao K, *Mat. Sc. and Tech.*, (22) 97-104(2006)
 32. Valérie Guillaumin and Georges Mankowski, *Corros. Sci.* 41(3) 421-438(1998)